East European Journal of Physics. **1.** 40-46 (2022)
DOI:10.26565/2312-4334-2022-1-06 ISSN 2312-4334

EFFECT OF THE RELATIVISTIC ELECTRON BEAM ON PROPAGATING WHISTLER-MODE WAVE FOR RING DISTRIBUTION IN THE SATURN MAGNETOSPHERE†

E.H. Annex[a,#], Rama S. Pandey[a,*], Mukesh Kumar[b,§]
[a]*Department of Applied Physics, Amity Institute of Applied Science, Amity University Noida UP India*
[b]*Department of Physics, Nalanda College Biharsharif Nalanda MU Bodh Gaya Bihar, India*
**Corresponding Author: rspandey@amity.edu*
[#]E-mail: annex.h@student.amity.edu; [§]E-mail: mukeshkumarpawapuri@gmail.com
Received February 10, 2022; accepted March 15, 2022

Cassini and many investigators reported whistler chorus near Saturn equatorial plane moving outwards. Whistler can propagate when going to high latitude and can alter its characteristics while interacting resonantly with available energetic electrons. Here investigating wave for a relativistic beam of the electron. It is observed and reported by Cassini Magnetospheric Imaging Instrument (MIMI) that inward radial injection of highly energetic particles is most dominant in Saturn intrinsic magnetosphere. Within this paradigm, an empirical energy dispersion relation for propagated whistler-mode oscillations in quasi Saturn magnetospheric plasma from such a non-monotonous ringed distribution function has been established. The kinetic approach and method of characteristics methodologies were used in the computations, which have been shown to be the best for building perturbed plasma states. The perturbed distribution function was estimated using the unperturbed particle routes. The ring distribution function was used to construct an unexpected growth rate expression for relativistic plasma in the inner magnetosphere. The results from the Saturn magnetosphere have been calculated and interpreted using a range of parameters. Temperature heterogeneity was shown to be a significant source of free energy that aided the propagation of a whistler-mode wave. By raising the peak value, the bulk injection of energetic hot electron injection impacts the growth rate. Growth was also demonstrated to be accelerated when the propagation angle increased. The research contributes to a better understanding of the relationship between wave and particle emissions and VLF emissions on a large scale.
Keywords: Magnetospheric environment of Saturn, rate of growth, wave-particle interactions, Whistler Mode Waves
PACS: 41.75Hf, 94.30Tz, 96.30Wr, 96.30Mh

Gurnett et al [1] were the first to report on the plasma spectrum detected by Voyager 1 on Saturn. Voyager found Whistler mode hissing and choral noises when it reached the equator at an inner radius of around 5 Rs (Rs is Saturn's radius). Voyager 2's plasma wave instruments detected Whistler mode pulses from Saturn's magnetosphere [2]. Gurnett et al [1] supplied the earliest Cassini and Plasma Waves Scientific Instrument information, along with Saturn's first orbit, during the 2005 approach. Some diffuse emissions (electron cyclotron frequency) were detected at frequencies lower than FC. Whistler mode wave emissions have been identified. The radial distance between these radiations ranges between 2 and 6 Rs. Whistler waves are electromagnetic waves that arise in magnetised plasma and have a lower frequency than the electron cyclotron frequency. The magnetosphere causes plasma instabilities, causing waves to move in the Whistler mode wave forks. Non-uniform electron distributions, such as beams, rings, and thermal anisotropy, produce the majority of these instabilities. Whistler's launch mode is also activated when it is created by lightning. The addition of relativistic energetic hot electrons in bulk alters the growth rate by raising its maximum value [3]. A crucial mechanism that might result in wave amplification and the precipitation of high-energy electrons as from magnetic region into the lower atmosphere is the interaction of Whistler mode wave particles. Cassini was the first spacecraft to arrive at Saturn in 2004. It has a wide radial cover of Saturn's ionosphere.

Understanding non-relativistic astrophysical shocks is a significant aspect toward Treumann's [4] general account of collisionless astrophysical shocks with high Mach numbers and their effects on dispersing flow-energy, heating matter, ramping up particles to high supposedly cosmic-ray energies, and generating distinguishable radiation varying from radio to X-rays. The waves, according to Sundkvist et al [5], are an important part of the shock structure, with the dispersive shock serving as the source of the waves by pushing the Poynting flux of the oblique whistler waves upstream in the shock normal frame commencing at the shock ramp.

Went et al. [6] presented a new analytical and numerical model of Saturn's dayside bow shock based on empirical evidence from the Pioneer 11, Voyager 1, and Voyager 2 flybys, as well as data from the first six years of the Cassini mission (2004–2010), in order to derive the average structure of the shock surface and the variance of shock sub solar distance with solar wind dynamic pressure. Wilson et al [7] started to investigate electromagnetic precursor waves, distinguished as whistler-mode waves at supercritical interplanetary shocks, which continue to spread obliquely about the local magnetic field, shock normal vector, and solar wind speed and are not phase standing structures, using the Wind search coil magnetometer.

Recently Sokolovsky [8] has been discussed the relaxation of the electron energy and momentum densities in spatially uniform states of completely ionized plasma in the presence of small constant and spatially homogeneous external electric field on based on linear kinetic equation obtained by us early from the Landau kinetic equation. Whistler-

† ***Cite as***: E.H. Annex, R.S. Pandey, and M. Kumar, East. Eur. J. Phys. **1**, 40 (2022), https://doi.org/10.26565/2312-4334-2022-1-06

mode waves are acknowledged to have a role in electron thermodynamics/acceleration and are identified as wave trains before the shock ramp under specified conditions by Sulaiman et al [9]. Sulaiman et al.[10] provided the parameter space of MA bow shock crossings detected by the Cassini probe from 2004 to 2014. We discover that Saturn's bow shock has properties similar to both terrestrial and astrophysical regimes (MA of order 100), which are primarily determined by the intensity of the upstream magnetic field. Sulaiman et al [11] researched the process thoroughly, both theoretically and through simulations, but their conclusions are few and few between. We examine extremely high Mach number events in previously unknown parameter space, and we use in situ magnetosphere data from the Cassini mission at 10 AU to investigate reformation.

GOVERNING DISPERSION RELATION

To get the dispersion relation, uniform anisotropy in space is used, as well as collision-free plasma hit by an external magnetic field with Bo = Bo êz. Inhomogeneities in the contact region are minor. Kaur and Pandey's [12] technical and geometric principles are being pursued. As a consequence of a long derivation, Kumari and Pandey[13] wrote the Vlasov equation – the Dielectric tensor from equation (14)

$$\varepsilon_{ij}\left(k,\omega\right)=1+\left\{\frac{4e_s^2\pi}{\left(\beta m_e\right)^2\omega^2}\right\}\int\frac{d^3P\sum_{i,j}^{x,y,z}\|S_{ij}^{*}\|}{\left(\omega-k_{\|}\frac{P_{\|}}{\beta m_e}-n\frac{\omega_{cs}}{\beta}\right)}. \tag{1}$$

For the parallel propagation and instability of whistler mode waves with $k_{\perp}=0$, the branch of general dispersion relation (1) reduces to:

$$\varepsilon_{xx}\pm i\varepsilon_{xy}=N^2, \tag{2}$$

where $N^2=\left(k^2c^2\right)\big/\omega^2$ is refractive index. As a result, the dispersion relation for n=1 may be stated as follows:

$$N^2=1+\frac{4e_s^2\pi}{\left(\beta m_e\right)^2\omega^2}\int\frac{d^3\mathbf{P}}{2}\mathbf{P}_{\perp}\left[N_1+N_2\right]\times\left[\frac{1}{\omega-\frac{k_{\|}\mathbf{P}_{\|}}{\beta m_e}\pm n\frac{\omega_c}{\beta}}\right], \tag{3}$$

where

$$N_1=\frac{\left(\beta m_e\right)^2}{\mathbf{P}_{\perp}}\frac{\partial f_o}{\partial\mathbf{P}_{\perp}}\left(\omega-\frac{k_{\|}\mathbf{P}_{\|}}{\beta m_e}\right)\left(\frac{\mathbf{P}_{\perp}}{\beta m_e}\right), \tag{4}$$

$$N_2=\beta m_e k_{\|}\frac{\partial f_o}{\partial\mathbf{P}_{\|}}\left(\frac{\mathbf{P}_{\perp}}{\beta m_e}\right). \tag{5}$$

The trapped electron distribution function is considered to be a Maxwellian ring momentum distribution function.

$$f(\mathbf{P}_{\perp},\mathbf{P}_{\|})=\frac{n_e/n}{\pi^{3/2}P_{o\|}P_{o\perp}^2B}\exp\left[-\frac{\left(\mathbf{P}_{\perp}-P_o\right)^2}{P_{o\perp}^2}-\frac{\left(\mathbf{P}_{\|}^2\right)}{P_{o\|}^2}\right], \tag{6}$$

$$B=\exp\left(-P_o^2/P_{o\perp}^2\right)+\sqrt{\pi}\left(\frac{P_o}{P_{o\perp}}\right)\operatorname{erfc}\left(-P_o/P_{o\|}\right), \tag{7}$$

where,

$$P_{o|}=\left(\frac{2k_bT_{\|}}{\beta m_e}\right)^{1/2}\text{ and }P_{o\perp}=\left(\frac{2k_bT_{\perp}}{\beta m_e}\right)^{1/2},$$

are the associated parallel and perpendicular electron thermal velocities.

Substituting $d^3\mathbf{P}=2\pi\int_0^{\infty}\mathbf{P}_{\perp}d\mathbf{P}_{\perp}\int_{-\infty}^{\infty}d\mathbf{P}_{\|}$ Then by plugging expression (6) into equation (3) and solving the integrations, we get the dispersion relation as follows:

$$\frac{k^2c^2}{\omega^2}=1+\frac{4\pi e_s^2}{\left(\beta m_e\right)\omega^2}\frac{\left(n_e/n\right)}{B}\left[X_1\frac{\beta m_e\omega}{k_{\|}P_{o\|}}Z\left(\xi\right)+X_2\left(1+\xi Z\left(\xi\right)\right)\right], \tag{8}$$

where $X_1=1+\frac{P_o^2}{P_{o\perp}^2}-\frac{P_o}{P_{o\perp}}\sqrt{\pi}$

$$X_2 = \left[X_1 + \frac{P_{o\perp}^2}{P_{o\|}^2}\left(1 - \sqrt{\pi}\frac{P_o^3}{P_{o\perp}^3}\mathrm{erf}\left(\frac{P_\perp'}{P_{o\perp}}\right) + 3\frac{P_o^2}{P_{o\perp}^2} - \frac{3}{2}\sqrt{\pi}\frac{P_o}{P_{o\perp}}\right)\right],$$

where

$Z(\xi) = \frac{1}{\sqrt{\pi}}\int_{-\infty}^{\infty}\frac{e^{-t^2}}{t-\xi}dt$, is the plasma dispersion function with $\xi = \frac{\beta m_e}{k_\| P_{o\|}}\left(\omega \mp \frac{\omega_c}{\beta}\right)$.

Applying condition $\frac{k^2c^2}{\omega^2} >> 1$ for whistler waves

$$\omega_{ps}^2 = \frac{4e^2\pi n_e/n}{B_o m_e}.$$

The equation (8) reduces to

$$D(k,w) = \frac{-k^2c^2}{\omega_{ps}^2} + \frac{1}{\beta}\left[\frac{X_1\omega}{k_\| P_{o\|}}(\beta m_e)\left\{-\frac{1}{\xi} - \frac{1}{2\xi^3}\right\} - \left\{X_2\frac{1}{2\xi^2}\right\} + \left[\frac{(\beta m_e)\omega}{k_\| P_{o\|}}X_1 + X_2\xi\right]\left\{i\sqrt{\pi}\exp\left(-\xi^2\right)\right\}\right]. \quad (9)$$

Introducing the dimensionless parameters as $\tilde{k} = \frac{k_\| P_{o\|}}{\omega_{cs}}$,

where $K_2 = \frac{1}{2X_1}$ and $\beta_1 = \frac{4\pi\mu_o\varepsilon_o k_b T_\| (n_e/n)}{m_e^2 B B_o^2}$.

Growth rate expression for oblique propagation

When Whistler mode wave propagate oblique to magnetic field direction, the expression of dimensionless growth rate and dimensionless real frequency becomes:

$$\frac{\gamma}{\omega_c} = \frac{\frac{\sqrt{\pi}}{\beta\tilde{k}\cos\theta}\left(\frac{X_2}{X_1} - \frac{\beta X_3}{1-\beta X_3}\right)(1-\beta X_3)^3\exp\left[-\left(\frac{1-\beta X_3}{\tilde{k}\cos\theta}\right)^2\right]}{1+\beta X_4 + \frac{(\tilde{k}\cos\theta)^2}{2(1-\beta X_3)^2} - \frac{(\tilde{k}\cos\theta)^2}{(1-\beta X_3)}\left(\frac{X_2}{X_1} - \frac{\beta X_3}{1-\beta X_3}\right)}, \quad (10)$$

$$X_3 = -\frac{\omega_r}{\omega_c} = \frac{(\tilde{k}\cos\theta)^2}{\beta_1}\left[K_2 + \frac{X_2}{X_1}\frac{\beta_1}{2\beta}\right]. \quad (11)$$

Expression for growth rate for parallel propagation

When Whistler mode wave propagate parallel to magnetic field direction, the expression of dimensionless growth rate and dimensionless real frequency becomes:

$$\frac{\gamma}{\omega_c} = \frac{\frac{\sqrt{\pi}}{\beta\tilde{k}}\left(\frac{X_2}{X_1} - \frac{\beta X_3}{1-\beta X_3}\right)(1-\beta X_3)^3\exp\left[-\left(\frac{1-\beta X_3}{\tilde{k}}\right)^2\right]}{1+\beta X_4 + \frac{(\tilde{k})^2}{2(1-\beta X_3)^2} - \frac{(\tilde{k})^2}{(1-\beta X_3)}\left(\frac{X_2}{X_1} - \frac{\beta X_3}{1-\beta X_3}\right)}, \quad (12)$$

$$X_3 = -\frac{\omega_r}{\omega_c} = \frac{(\tilde{k})^2}{\beta_1}\left[K_2 + \frac{X_2}{X_1}\frac{\beta_1}{2\beta}\right]. \quad (13)$$

Plasma Parameters

The estimation of the growth rate of Whistler mode waves at radial distances was validated using characteristics from Voyager 1 and Cassini data [12,13] at R ~ 5Rs within the Saturn plasma sheet. For a radial distance of 5Rs, the magnetic field strength is 184 nT and the number density is 5×107 m^{-3}. Energy density $K_B T_\|$ According to observation, the energy density at R ~ 5Rs is 300 eV.

RESULT AND DISCUSSION

In Fig. 1 the maximum growth rate shows for A_T =0.75, and reaches up to 4, other profiles of A_T =0.5 and A_T = 0.25 shows same pattern of growth rate but significantly low maxima 3.6 and 3.25 for A_T = 0.5 and A_T = 0.25 respectively.

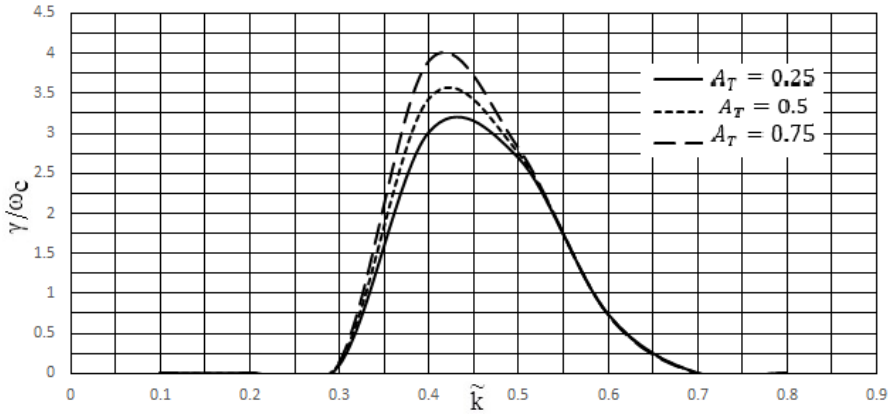

Figure 1. Variation in the pace of growth and actual frequencies in relationship to $\tilde{k}$ for various values of A_T for $\theta = 10^o$ at, n_o=5x10^{5}m^{-3},$n_c/n_w = 1/10$, $P\_0 = 0.2$, and as well as other fixed plasma characteristics

The increasing growth rate is of same pattern with substantial increment in the growth rate. But the decreasing pattern it follows same path below 2.75 and ends in $\tilde{k}$ value of 0.7. The variation in growth rate with regard to wave number for various values of temperature anisotropy has recently been shown. According to the dispersion relation, when temperature anisotropy grows, the growth rate increases in both sense, frequency, and magnitude due to the presence of a hot ring's electron and a cool electron around it. Maniitti et al.[14] found an increase in whistler owing to an increase in temperature ratio. In Fig. 2 the maximum growth rate for θ=30, reaches up to 4.25 for a $\tilde{k}$ value of 0.4, other profiles of θ=20 and θ =10 shows same pattern of growth rate but significantly low maxima 4 and 3.25 respectively.

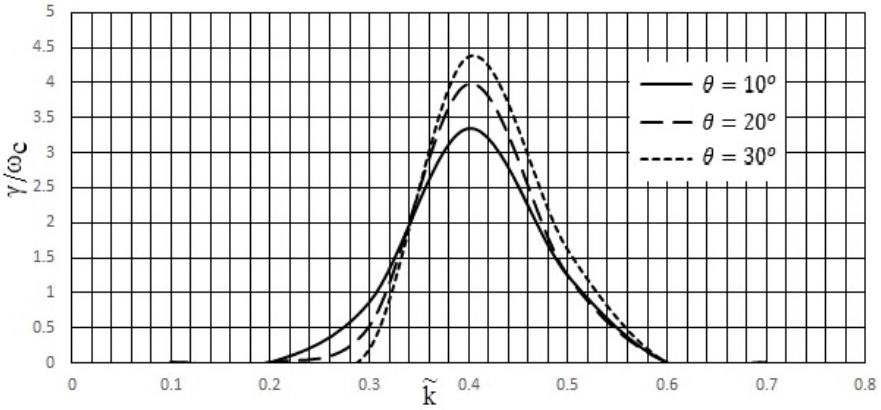

Figure 2. Variation in the pace of growth and actual frequencies in relationship to $\tilde{k}$ for various values of θ for at $K_B T_{||}$=2KeV, $T_{\parallel}/T_{\perp} = 1.5$, n_o=5x10^{5}m^{-3},$n_c/n_w = 1/10$, $P\_0 = 0.2$, as well as other fixed plasma characteristics.

The growing growth rate follows the same trend, with a significant increase in the growth rate. The variation in growth rate with regard to wavenumber has been demonstrated for various propagation angle values. It has been revealed that increasing the propagation angle value increases the growth rate. Fig. 3: With a $\tilde{k}$ value of 0.8, the maximum growth rate for =0.5 is achieved.

And the maximum growth rate for β=0.6, reaches maximum at a $\tilde{k}$ value of 0.84 Similarly, the maximum growth rate for β=0.7, reaches maximum at a $\tilde{k}$ value of 0.72. β=0.5 curve shows a phenomenal growth rate than the β=0.6 and β=0.7. as compared to the β=0.5 other curves are shallow. In terms of wavenumber, raising the value of relativistic factor leads in a decreasing growth rate, i.e., the greatest peak occurs for the lowest value. Similarly, at higher velocity of highly energetic particles, smaller is measured, signifying more expansion of whistlers. Thus, while this cannot be referred to as the key component responsible for whistler expansion in particle ring distributions, it can be substantial in other types of distributions such as Maxwellian [15]. In Fig. 4 the maximum growth rate for $n_c/n_w = 1/10$, reaches maximum at a $\tilde{k}$ value of 0.5 And the maximum growth rate for $n_c/n_w = 1/20$, reaches maximum at a $\tilde{k}$ value of 0.4 Similarly, the maximum growth rate $n_c/n_w = 1/30$,reaches maximum at a $\tilde{k}$ value of 0.4. The growing growth rate follows the same trend, with a significant increase in the growth rate. the variation in growth rate caused by relativistic warm electrons, i.e., nc/nw. The graphic clearly shows that the growing ratio of number density causes an increase in growth rate.

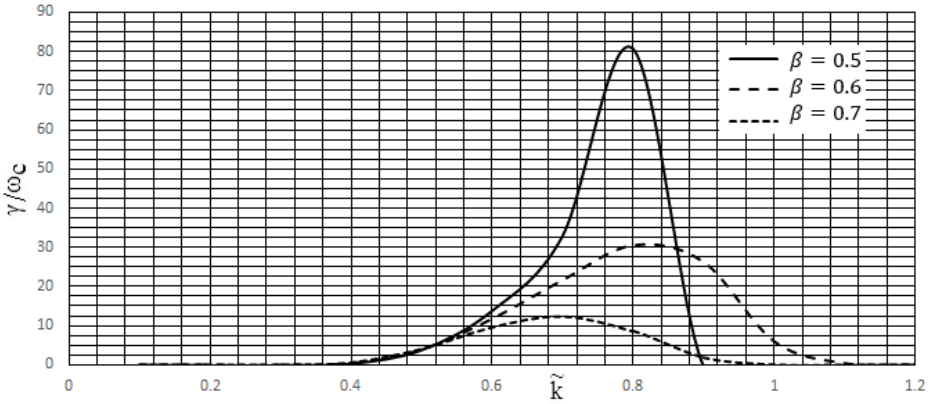

Figure 3. Variation in the pace of growth and actual frequencies in relationship to $\tilde{k}$ for various values of β for $\theta = 10^{o}$ at $K_B T_{||}$=2KeV, $T_{\|}/T_{\perp} = 1.5$, n_o=5x10^{5}m^{-3},$n_c/n_w = 1/10$, $P\_0 = 0.2$, as well as other fixed plasma characteristics.

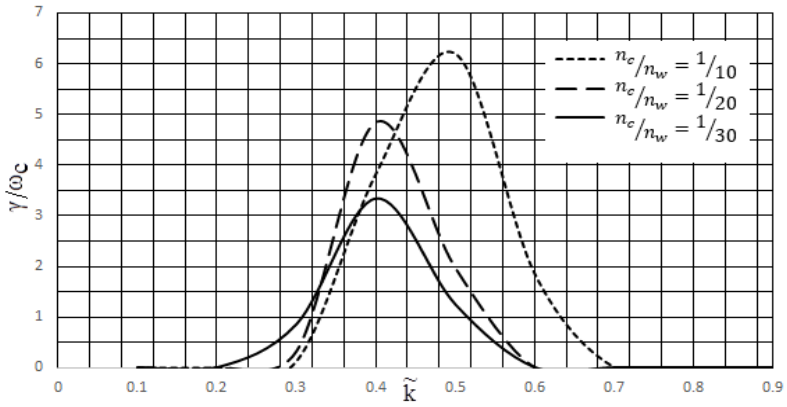

Figure 4. Variation in the pace of growth and actual frequencies in relationship to $\tilde{k}$ for various values of $^{n_c}/_{n_w}$ for $\theta = 10^{o}$ at, n_o=5x10^{5}m^{-3},$n_c/n_w = 1/10$, $P\_0 = 0.2$, as well as other fixed plasma characteristics.

Fig. 5: The maximum growth rate for $n_c/n_w = 1/10$, reaches maximum at a $\tilde{k}$ value of 0.4 And the maximum growth rate for $n_c/n_w = 1/20$, reaches maximum at a $\tilde{k}$ value of 0.4 Similarly, the maximum growth rate $n_c/n_w = 1/30$, reaches maximum at a $\tilde{k}$ value of 0.4.

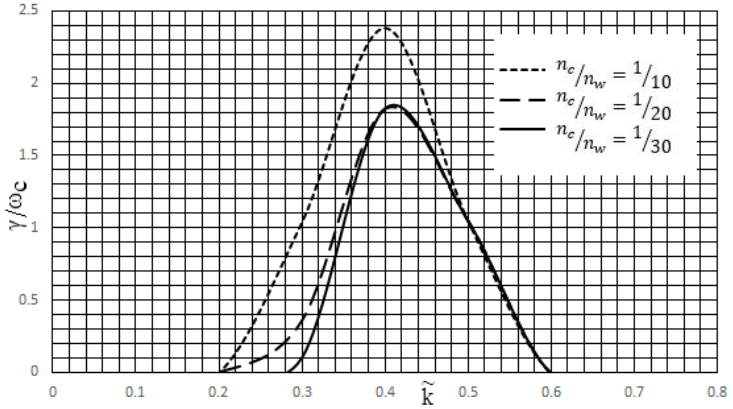

Figure 5. Variation in the pace of growth and actual frequencies in relationship to $\tilde{k}$ for various values of $^{n_c}/_{n_w}$ for *parallel beam* at, $P\_0 = 0.2$, $K_B T_{||}$=2keV, $A_T = 0.75$,$\beta = 0.7$ as well as other fixed plasma characteristics.

Growth rate builds up for a $\tilde{k}$ value of 0.2 and 0.3 where $n_c/n_w = 1/20$ and $1/30$ respectively. Both the curves reaches a maximum at a $\tilde{k}$ value of 0.4 and decays to a $\tilde{k}$ value of 0.6. Fig. 6: The maximum growth rate shows for A_T =0.75, reaches a maximum at a $\tilde{k}$ value of 0.4, other profiles of A_T =0.5 and A_T =0.25 shows same pattern of growth rate. At A_T =0.5 and A_T =0.25 the $\tilde{k}$ value reaches a maximum of 0.4. All the three curves decays to a same point at a $\tilde{k}$ value of 0.6. the growth curve are of similar in nature but the A_T =0.75 growth is higher than all other two values. In the incremental phase the growth pattern is different but the decremental phase falls in the same pattern. Fig. 7: The highest growth rate for = 0.5 occurs with $\tilde{k}$ value of 0.72. And the greatest growth rate for =0.6 occurs with $\tilde{k}$ value of 0.62.

Similarly, the maximum growth rate for =0.7 is reached at $\tilde{k}$ = 0.58. The three curves begin at the same place with $\tilde{k}$ value of 0.32 and decline at various $\tilde{k}$ values.

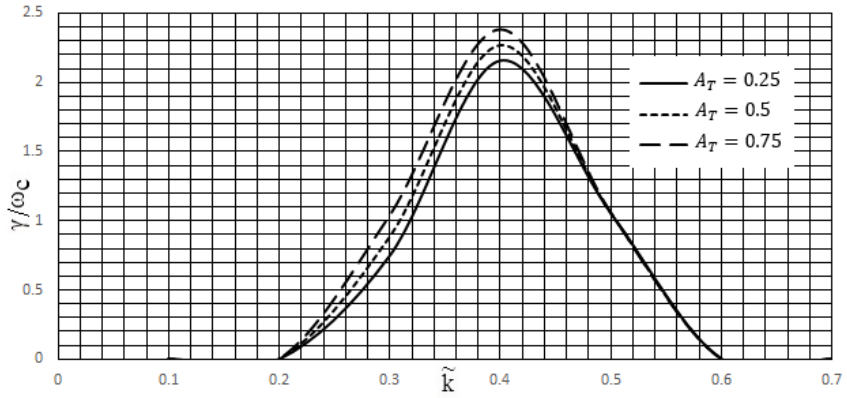

Figure 6. Variation in the pace of growth and actual frequencies in relationship to $\tilde{k}$ for various values of A_T for *parallel beam* at, $P\_0 = 0.2$, $K_B T_{||}$=2keV, $\beta = 0.7$ as well as other fixed plasma characteristics.

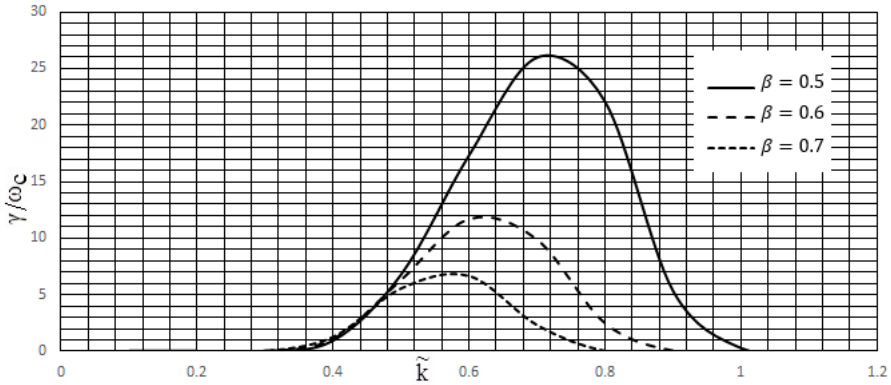

Figure 7. Variation in the pace of growth and actual frequencies in relationship to $\tilde{k}$ for various values of β for *parallel beam* at, $P\_0 = 0.2$, $K_B T_{||}$=2keV, $A_T = 0.75$ as well as other fixed plasma characteristics.

CONCLUSION

The influence of temperature anisotropy and relativistic beam characteristics on the evolution of whistler-mode waveforms in the Saturnian magnetosphere is explored, and these qualities are shown to be favourable. The rate of growth slows as the value of temperature anisotropy rises, but it accelerates when the AC frequency rises. As the propagation angle rises, so does the bandwidth of oblique propagation. By assuming that electrons are the major high energy particles influenced by electromagnetic activity in the magnetospheres of other planets, the preceding results help us comprehend the character of this unpredictable whistler-mode wave scenarios [16].

ORCID IDs

E.H. Annex, https://orcid.org/0000-0002-5193-6795; **Rama S. Pandey,** https://orcid.org/0000-0003-4907-1080;
Mukesh Kumar, https://orcid.org/0000-0001-6106-4794

REFERENCES

[1] D.A. Gurnett, W.S. Kurth, and F.L. Scarf, Science, **212**, 235 (1981), https://doi.org/10.1126/science.212.4491.235
[2] F.L. Scarf, D.A. Gurnett, W.S. Kurth, and R.L. Poynter, **215**, 587 (1982), https://doi.org/10.1126/science.215.4532.587
[3] S. Kumar, S.K. Singh, and A.K. Gwal, Pramana J. Phys. **68**(4), 611 (2007), https://doi.org/10.1007/s12043-007-0063-z
[4] R.A. Treumann, Astron. Astrophys. Rev. **17**, 409 (2009), https://doi.org/10.1007/s00159-009-0024-2
[5] D. Sundkvist, V. Krasnoselskikh, S.D. Bale, S.J. Schwartz, J. Soucek, and F. Mozer, Phys. Rev. Lett. **108**, 2 (2012), https://doi.org/10.1103/PhysRevLett.108.025002
[6] D.R. Went, G.B. Hospodarsky, A. Masters, K.C. Hansen, and M.K. Dougherty, J. Geophys. Res. **116**, A07202, (2011), https://doi.org/10.1029/2010JA016349
[7] L.B. Wilson, A. Koval, A. Szabo, A. Breneman, C.A. Cattell, K. Goetz, P.J. Kellogg, K. Kersten, J.C. Kasper, B.A. Maruca, and M. Pulupa, Geophys. Res. Lett. **39**, L08109 (2012), https://doi.org/.1029/2012GL051581
[8] A.I. Sokolovsky, S.A. Sokolovsky, and O.A. Hrinishyn, East European Journal of Physics, **3**, 19, (2020), https://doi.org/10.26565/2312-4334-2020-3-03
[9] A.H. Sulaiman, D.A. Gurnett, J.S. Halekas, J.N. Yates, W.S. Kurth, and M.K. Dougherty, **122**(1), 227 (2017) https://doi.org/10.1002/2016JA023501

[10] A.H. Sulaiman, et al. J. Geophys. Res. **121**, 4425 (2016), https://doi.org/10.1002/2016JA022449
[11] A.H. Sulaiman, et al. Phys. Rev. Lett. **115**, 12 (2015), https://doi.org/10.1103/PhysRevLett.115.125001
[12] R. Kaur, and R. S. Pandey, Adv. Space Res. **59**, 2434 (2017), https://doi.org/10.1016/j.asr.2017.02.015
[13] J. Kumari, and R.S. Pandey, J. Astrophys. Astr. **40**, 14 (2019), https://doi.org/10.1007/s12036-019-9576-3
[14] J.D. Menietti, O. Santolík, and M.K. Dougherty, J. Geophys. Res. **113**, A12206 (2008), https://doi.org/10.1029/2008JA013237
[15] Y. Omura, and D.J. Summers, Geophys. Res. **111**, A09222 (2006), https://doi.org/101029/2006JA011600
[16] C.S. Wu, P.H. Yoon, and H.P. Freund, Geophys. Res. Lett. **16**(12), 1461 (1989), https://doi.org/10.1029/GL016i012p01461

ВПЛИВ РЕЛЯТИВІСТСЬКОГО ЕЛЕКТРОННОГО ПРОМЕНЯ НА ПОШИРЕННЯ ХВИЛЬ З ВІСТЛЕРНИМИ МОДАМИ ДЛЯ КІЛЬЦЕВОГО РОЗПОДІЛУ В МАГНІТОСФЕРІ САТУРНА

Є.Х. Аннекс, Рама С. Пандей, Мукеш Кумар
[a]*Факультет прикладної фізики, Інститут прикладних наук Аміті, Університет Аміті, Нойда UP, Індія*
[b]*Факультет фізики, Наланда Коледж, Біхаршаріф Наланда, Бодх Гайя Біхар, Індія*

Кассіні та багато дослідників повідомили, що whistler хор поблизу екваторіальної площини Сатурна рухається за його межі. Він може поширюватися, коли піднімається у високі широти, і може змінювати свої характеристики, резонансно взаємодіючи з доступними енергійними електронами. У статті досліджується хвиля для релятивістського електронного променя. За допомогою Cassini Magnetosphere Imaging Instrument (MIMI) спостерігається та повідомляється, що радіальна інжекція високоенергетичних частинок всередину є найбільш домінуючим у внутрішній магнітосфері Сатурна. В рамках цієї парадигми було встановлено емпіричне співвідношення дисперсії енергії для поширюваних коливань вістлерної моди в квазісатурновій магнітосферній плазмі від такої немонотонної кільцевої функції розподілу. У розрахунках використано кінетичний підхід та методику характеристик, які виявилися найкращими для побудови збурених станів плазми. Збурену функцію розподілу оцінили з використанням маршрутів незбурених частинок. Кільцева функція розподілу була використана для побудови виразу неочікуваної швидкості зростання релятивістської плазми у внутрішній магнітосфері. Результати для магнітосфери Сатурна були розраховані та інтерпретовані з використанням ряду параметрів. Було показано, що температурна неоднорідність є значним джерелом вільної енергії, яка сприяє поширенню хвилі вістлерної моди. Підвищуючи пікове значення, об'ємна інжекція енергетичних гарячих електронів впливає на швидкість росту. Було також продемонстровано, що зростання прискорюється при збільшенні кута поширення. Дослідження сприяє кращому розумінню зв'язку між випромінюваннями хвиль і частинок і VLF-випромінюванням у великому масштабі.

Ключові слова: магнітосферне середовище Сатурна, швидкість росту, взаємодія хвиля-частинка, хвилі моди Уістлера